# Flood forecast with chained hydrologic-hydraulic modelling and data assimilation

Thanh Huy Nguyen[1,2], Andrea Piacentini[1], Simon Munier[3], Sophie Ricci[1,2], Raquel Rodriguez Suquet[4], Sophie Le Gac[4], Francois Boy[4], Christophe Fatras[5], Quentin Bonassies[1,2], Malak Sadki[1,2], Santiago Pena Luque[4]
[1] CERFACS, Toulouse, 31057, France
[2] CECI, CERFACS/CNRS UMR 5318, Toulouse, 31057, France
[3] Centre National de Recherches Météorologiques (CNRM), Toulouse, 31057, France
[4] Centre National d'Etudes Spatiales (CNES), Toulouse, 31401, France
[5] Collecte Localisation Satellites (CLS), 31520, Ramonville Saint-Agne, France
thnguyen@cerfacs.fr

***Abstract* – Early warning and prediction of flood events have become all the more essential as the occurrence and intensity of flooding have increased in recent decades. In this work, the upstream boundary condition for a local-scale hydrodynamic TELEMAC-2D (T2D) model is provided by the outputs of a large-scale hydrologic model ISBA-CTRIP. The studied test case is the Garonne Marmandaise catchment (southwest of France), that is prone to flooding, with a focus on a medium-sized flood event that occurred in January-March 2022. To account for the uncertainties related to the inflow provided by ISBA-CTRIP as well as the friction coefficients and hydraulic state, we focus on the assimilation of remote-sensing flood observations, namely longitudinal river water surface elevation (WSE) profiles provided by Sentinel-6MF altimetry data, and 2D flood extent observations derived from Sentinel-1 SAR images acquired during overflowing events. An Ensemble Kalman Filter (EnKF) with a dual state-parameter data assimilation (DA) approach is implemented on top of the T2D model. The observation operator associated with the longitudinal river WSE profiles and the water surface ratio (WSR) observations, as well as the dual state-parameter sequential correction, were implemented and validated. This work paves the way toward a cost-effective and reliable methodology for flood forecasting and flood risk assessment that allows moving towards a perspective working with poorly-gauged or ungauged catchments.**

***Keywords***: Flooding, data assimilation, ensemble Kalman Filter, remote sensing, Garonne.

## I. INTRODUCTION

Flooding is one of the most common and costliest natural disasters worldwide in recent decades. In the context of operational flood forecasting, the challenges lie in producing reliable forecasts given constrained computational resources and within processing time that is compatible with real-time forecasting. Flood hydrodynamic models typically depend on observed data from gauge networks, e.g., water level and/or discharge that describe the forcing time-series at the upstream and lateral boundary conditions (BCs) of the model. However, this information is not always available, due to a lack of in-situ gauge data—which is declining worldwide [1]—or because the stream gauge measurements acquired during high-overflowing periods are unreliable. Additionally, in order to reach longer forecast lead times, a forecasted inflow discharge should be described, e.g., discharge simulated by large-scale hydrologic models [2].

While hydrologic and hydraulic numerical models play an essential role in flood forecasting, their capabilities remain limited due to uncertainties in their input data such as rainfall, inflow, geometry and topography of the catchment and the river (e.g., topographic and bathymetric errors from Digital Elevation Models (DEMs)), as well as hydraulic parameters (calibration of friction coefficients). As a result, data assimilation (DA) prevails as an efficient tool to reduce these uncertainties, by combining numerical model outputs with various Earth Observations from space or from in-situ stream gauge measurements. In this regard, the volume of data from space missions have been increasing considerably in recent years. They provide heterogeneous and relevant data such as altimetry (Sentinel-6, SWOT), optical (Sentinel-2, Pléiades) and radar (Sentinel-1, TerraSAR-X). In particular, Synthetic Aperture Radar (SAR) is capable of all-weather global imagery of continental waters, which are depicted by low backscatter pixels resulting from the specular reflection of the radar pulses upon their incidence against the water surfaces. Based on such information, our previous studies [3, 4, 5] have focused on the assimilation of wet surface ratio (WSR) derived from Sentinel-1 (S1) SAR images, in addition to in-situ water level data. As such, an ensemble DA approach has been developed to accommodate these 2D WSR observations alongside in-situ water level time-series within an Ensemble Kalman Filter (EnKF) framework has been implemented on the TELEMAC-2D (T2D) hydrodynamic model set up over the Garonne Marmandaise catchment.

In this work, we focus on the usage of remote sensing data and the improvement of flood forecasting relying on only this data, compared to the conventional method that uses only in-situ data. The merits of such DA methods (both the one using only in-situ and only RS data) are demonstrated in the high uncertainty conditions. Indeed, the upstream BC of the T2D model is provided by the large-scale hydrologic ISBA-CTRIP model [6], with the purpose of extending forecast lead time beyond the hydraulic network transfer time. As such, this work aims at near real-time flood forecasting by making the most out of the large volume of heterogeneous data from space.

## II. Study Area and Models

Free-surface hydraulic modelling is mainly governed by the Shallow Water equations (SWE), also known as Saint Venant equations derived from Navier-Stokes Equations. They express mass and momentum conservation averaged in the vertical dimension. In this work, the hydrodynamic numerical model TELEMAC-2D is used to simulate and predict the water level (denoted by $H$ [m]) and velocity (with horizontal components denoted by $u$ and $v$ [m.s$^{-1}$]) from which flood risks can be assessed effectively. It solves the SWE with an explicit first-order time integration scheme, a finite-element scheme and an iterative conjugate gradient method. A complete description of the underlying theoretical approach is provided in [7].

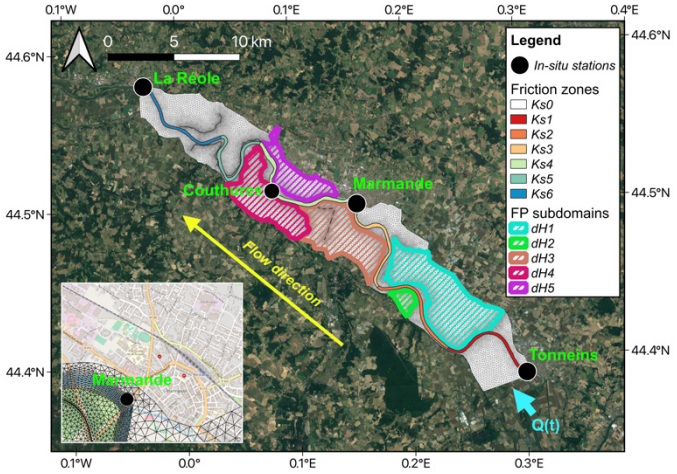



Figure 1. TELEMAC-2D Garonne Marmandaise model and control vector [3]. Inset figure magnifies the impacted urban area around Marmande.

The study area is the Garonne Marmandaise catchment (southwest France) which extends over a 50-km reach of the Garonne River between Tonneins and La Réole (Figure 1). This catchment has been equipped with hydraulic infrastructures, and a progressively constructed system of dykes and weirs to protect the floodplains from flooding events such as the historic flood of 1875 and to manage submersion and flood retention areas. Over this catchment, observing in-situ stations operated by the VigiCrue network (https://www.vigicrues.gouv.fr/) can be found at Tonneins, Marmande, and La Réole (black solid circles). In 2021, an additional station was installed by Vortex.io (https://www.vortex-io.fr/) at Couthures-sur-Garonne, henceforth called Couthures for short, to provide additional observations following the January-February 2021 major flood event occurred on this catchment. In this work, we focus on the flood event that occurred in December 2021 - January 2022. In-situ WL measured every 15 minutes during this flood event at Tonneins (blue line), Marmande (orange line), and La Réole (green line), and at Couthures (cyan line), are shown in Figure 2. Vertical lines stand for the overpass time of the Sentinel-1 (in grey/yellow dash-dotted lines for S1A and S1B, respectively) and Sentinel-6 (cyan dotted lines).

The large-scale hydrologic model ISBA-CTRIP [8] consists in the coupling between the ISBA land surface model (LSM) [9] and the CNRM-modified version of the TRIP river routing model (RRM) [10]. While ISBA simulates the exchanges of heat and water balance at the soil-atmosphere-vegetation and hydrology (i.e., surface and deep run-off) interfaces, CTRIP deals with the lateral transfer of freshwater towards the continent-ocean interface. Regarding the spatial resolution, the ISBA model is defined at global scale on a 0.5°×0.5° regular grid. On such a grid, the energy and water budget over continental surfaces are established, considering a three-layer soil. ISBA provides a diagnostic of the surface runoff and the gravitational drainage (i.e., water percolating to the deep layers of the soil), later used as forcing inputs for the RRM. On the other hand, the CTRIP model is defined on a regular latitude-longitude grid at an improved 1/12° resolution and it follows a river network to transfer water laterally from one cell to another, down to the interface with the ocean. This present work takes advantage of the recent CTRIP version from [8, 11] with a gridded map of discharge. The uncertainties in these simulated discharges mainly stem from uncertainties in the LSM inputs (i.e., precipitation), RRM parameters and catchment description.

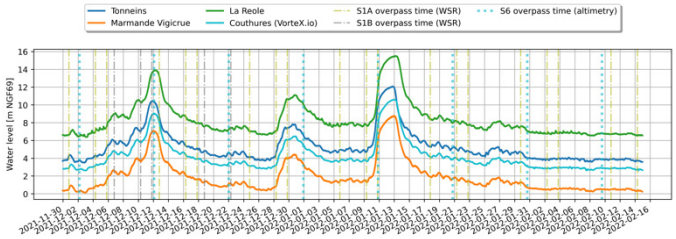



Figure 2. Water level time series at VigiCrue and Vortex.io observing stations, as well as S1 and S6 overpass times.

The TELEMAC-2D model over the Garonne Marmandaise catchment was developed and calibrated by EDF R&D [12]. It was built on a mesh of 41,000 nodes based on existing bathymetric cross-sectional profiles and topographic data [12]. A local rating curve at Tonneins is used to translate the observed WLs into a discharge time-series that is applied over the whole upstream interface (cyan arrow in Figure 1), including both river bed and floodplain boundary cells. Such a modelling strategy was implemented in order to cold start the T2D model with any inflow value. However, it prompts an artificial over-flooding over the upstream first meander, which would remain for a small period of time until the water returns to the river bed. On the other hand, the downstream BC at La Réole is described with a local rating curve built from gauge measurements. Over the simulation domain, the friction Strickler coefficient [13] is defined over seven zones, $Ks_1$ to $Ks_6$ for different segments of the river bed and $Ks_0$ for the entire floodplain. They are illustrated in Figure 1 by solid-coloured segments of the river bed and white region for the floodplain. It is worth noting that the description of friction coefficients is highly prone to uncertainties related to the zoning assumption, the calibration procedure, and the set of calibration events. In the absence of in-situ data in every river segment, their a priori values are set based on the calibration process from the original setting by EDF [12].

In addition, in order to account for the evapotranspiration, ground infiltration and rainfall processes that are lacking in the TELEMAC-2D Garonne model, a state correction in the floodplain has been implemented. Five subdomains delineated in the floodplain, represented by hatched coloured regions in

Figure 1 which involve a uniform WL correction over each subdomain, are added to the control vector. These state corrections are considered as zero-mean gaussian random vectors. These zones were determined based on the description of the storage areas [12] and the dyke system of the catchment. It is worth-noting that the first storage area of the model, at the first meander near Tonneins, is excluded in this study because of the aforementioned artificial over-flooding effect. In addition, several storage areas within the downstream region are not considered either, because they are not fully observed by S1, and some spurious dynamics may be caused by the errors in topography near La Réole [12]. Over each of the five zones, the ratio between the area of wet surfaces (observed by S1 images) and the total area of the subdomain is computed to provide observations in the floodplain.

In addition to the S1-derived flood extend observations, we also leverage data from a recent altimetry satellite, namely Sentinel-6-Michael Freilich (S6) [14]. These data were processed with Fully-focused SAR [15] allowing, for every S6 overpass, a profile of water surface elevation every 10 m along the river centreline. For this studied catchment, the S6 observations cover a similar area to that of the $Ks_2$ and $Ks_3$ friction coefficient of the riverbed. These relevant observations are taken advantage of in order to improve the performance of flood forecasting when relying on only remote-sensing data, compared to the conventional method that uses only in-situ data.

## III. METHOD

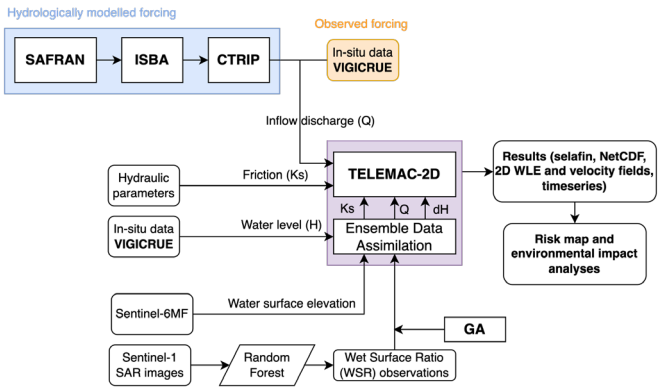



Figure 3. Overview workflow.

The general workflow for this study is illustrated in Figure 3. As aforementioned, the chained multi-physics and multi-scales modelling approach involves a direct supply of discharge forcing data for the T2D hydraulic model by a hydrologic model (blue block in Figure 3), instead of an observed streamflow from an in-situ gauging station (orange block in Figure 3). A similar approach was carried out between T2D and the large-scale RAPID hydrologic model within a twin experiment setup [2]. Here, the differences between two discharge time-series, respectively in blue and orange lines, are depicted by Figure 4, which shows the underestimated discharges with shortened duration over several peaks of the studied flood event. There are also a few days with low regimes where ISBA-CTRIP discharge is a little higher than the observed discharge, e.g., before the third peak of the flood event.

### A. Data assimilation

Figure 2 depicted all the data used in this work. The WL time-series at the three VigiCrue stations (Tonneins, Marmande and La Réole) as well as the S6 river WSE profiles and the S1-derived WSR computed over the five floodplain zones, are assimilated with the EnKF algorithm implemented on the TELEMAC-2D Garonne model (purple box in Figure 3). This allows for a sequential correction of the friction, the inflow discharge, and water level averaged over selected subdomains of the floodplain. The WL time-series observed at Couthures is used for validation only. Moreover, the WSR observations derived from S1 flood extent maps, being a ratio and non-gaussian, require a special treatment called Gaussian anamorphosis (GA) to be rendered into gaussian variables that are more compatible and optimal for the EnKF. The full description of the performed cycled EnKF algorithm and the applied GA can be found in [3, 5, 16, 17].

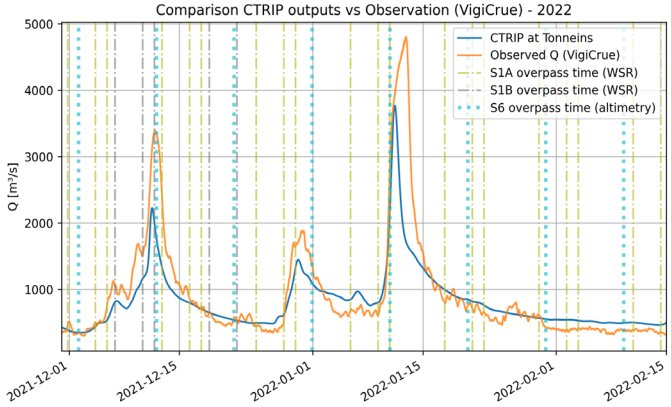



Figure 4. ISBA-CTRIP discharge (blue line) and observed discharge (orange line) time-series at Tonneins over the 2021-2022 flood event.

The observation error, for the computation of the corresponding covariance matrix R, is set proportional to the value of the in-situ WL observations (i.e., 10%) and to that of the WSE observations along the river centreline (i.e., 15%), whereas it is prescribed as a scalar fixed value for the WSR observations. The standard deviation of the S1-derived WSR observations is fixed to 0.1 (and up to 0.2 depending on how early the observation time within each assimilation window). These values stem from the assessment of the flood mapping algorithm that provides the wet/dry classification results (validated on five test sites all over the world) with an overall accuracy of 86.86% [16]. In addition, as opposed to [16], here no model-observation bias was taken into account for the in-situ WL data. All DA experiments were carried out using 75 members.

### B. Control vector

Table I summarises the variables included in the control vector of the performed EnKF. The friction coefficients are considered as random variables with a gaussian Probability Density Function (PDF) with mean and standard deviation estimated from the calibration process. The uncertainty in the upstream BC is also taken into account in order to address the

underestimated discharge provided by the hydrologic ISBA-CTRIP model. Therefore, a multiplicative factor $\mu$ applied on the time-dependent discharge time-series is considered as a random variable with a gaussian PDF centred at 1. In addition, the WL corrections applied uniformly on each of the five selected subdomains are denoted $\delta H_{1\text{-}5}$. They are considered as zero-mean gaussian random vectors.

Table I Gaussian PDF of uncertain input variables.

| Variables | Unit | Calibrated/ default value $x_0$ | Standard deviation $\sigma_0$ | 95% confidence interval |
|---|---|---|---|---|
| $Ks_0$ | $m^{1/3}s^{-1}$ | 17 | 0.85 | 17 ± 1.67 |
| $Ks_1$ | $m^{1/3}s^{-1}$ | 45 | 2.25 | 45 ± 4.41 |
| $Ks_2$, $Ks_3$ | $m^{1/3}s^{-1}$ | 38 | 1.9 | 38 ± 3.72 |
| $Ks_4$, $Ks_5$, $Ks_6$ | $m^{1/3}s^{-1}$ | 40 | 2.0 | 40 ± 3.92 |
| $\mu$ | - | 1 | 0.06 | 1 ± 0.0136 |
| $\delta H_{1..5}$ | m | 0 | 0.25 | 0 ± 0.0566 |

### C. Experimental setup

Three experiments were carried out, one in open-loop (OL) mode and two in DA mode. The first DA experiment involves only in-situ data assimilation (hence named IDA) as in conventional research works, whereas the second DA assimilates only RS observations (so-called RSDA). The three experiments are fed with the upstream BC provided by the ISBA-CTRIP discharge (blue line in Figure 4). In this work, the observed discharge was not used as forcing data for the experiments, it only serves as a reference for the ISBA-CTRIP discharge. The IDA experiment focuses on the sequential correction of friction coefficients and inflow discharge. Additionally, the RSDA experiment treats the hydraulic state variable in five floodplain subdomains, representing evapotranspiration and ground infiltration processes that are unavailable in the T2D Garonne model. The DA experiments were implemented with a cycled EnKF with an 18-hour assimilation window sliding with 6-hour overlapping. The simulation results were comprehensively assessed with 1D and 2D metrics with respect to the observations.

Table II Summary of the Free Run and DA experiment settings.

| Exp. | DA? | Assimilated observations | Nb of members | Control variables |
|---|---|---|---|---|
| OL | No | - | 1 | - |
| IDA | Yes | In-situ WSE | 75 | $Ks_{0..6}$, $\mu$ |
| RSDA | Yes | S1 WSR + S6 WSE | 75 | $Ks_{0..6}$, $\mu$, $\delta H_{1..5}$ |

## IV. Experimental Results

In this section, quantitative performance assessments are carried out in the control and in the observation spaces by:

(i) comparing the parameters yielded by the different DA analyses (subsection IV-A);
(ii) comparing the different analysed WL time-series with observations at in-situ observing stations, or along the river centreline at S6 dates (subsection IV-B and IV-C);
(iii) comparing the different analysed WSR with S1-derived WSR observations in the floodplain (subsection IV-D);

### A. Results in the control space

The analysed parameters from the two DA experiments are shown in Figure 5. The horizontal dashed lines stand for the default values (Table 1) which were used for the OL experiment, whereas the orange curves show the parameters of IDA (assimilating only in-situ data), and those of RSDA (assimilating only RS data) are represented by the green curves. Vertical lines represent the observation time of the S1 (grey/yellow dash-dotted lines) and S6 (cyan dotted lines), providing WSR observations over the floodplain and WSE at river centreline, respectively, that are altogether assimilated in the RSDA experiment.

Panels from the left column of Figure 5 show the friction coefficient in the floodplain $Ks_0$ and in the riverbed $Ks_{1\text{-}6}$. Since RSDA only assimilated remote-sensing data, its parameters have been corrected fewer times over the flood event compared to IDA. This is because the friction and inflow parameters stay constant within a DA cycle and if no observation was available during a cycle, they would remain the same from the previous cycle. On the other hand, the assimilation of in-situ data leads to many parameters to change significantly from the default/calibrated values and with a large variance between 20 and 70 $m^{1/3}s^{-1}$.

The first panel on the right column (Figure 5) presents the multiplicative factor $\mu$ obtained from the analyses. The resulting $\mu$ from IDA fluctuates considerably due to a potential equifinality when $\mu$ is combined with the friction coefficients in the control vector. On the other hand, RSDA-analysed parameter $\mu$ remains mostly more than one, showing the need to have more water into the catchment to account for the low ISBA-CTRIP discharge. Second to sixth panel from the right column of Figure 5 reveals the hydraulic state corrections $\delta H_{1\text{-}5}$. They are strictly negative in all five floodplain subdomains. This is because the flood event is not a major one with relatively mild overflowing, thus the observed flood extent maps are not prevailing, with most days showing little to no water detected in the floodplain. It leads to the δH trying to empty the floodplain.

Last panel shows the reconstructed upstream inflow discharge, i.e., the ISBA-CTRIP output multiplied by the analysed factor $\mu$ from the two DA experiments (orange: IDA, green: RSDA), in comparison to the observed discharge (black-dashed line). With the information from either in-situ data (IDA) and S6-derived WSE along the river centreline (RSDA) the flood peak discharge has been improved to match the same height as the observed discharge, however the phase delay remains unresolved. The evaluation of the DA experiments, in the control space for a real event, does not involve quantitatively assessing the performance of DA strategies, as the true values of the controlled parameters are unknown. Nevertheless, based on this diagnosis, it should be noted that there are potential equifinality issues here when only one type of observation was assimilated.

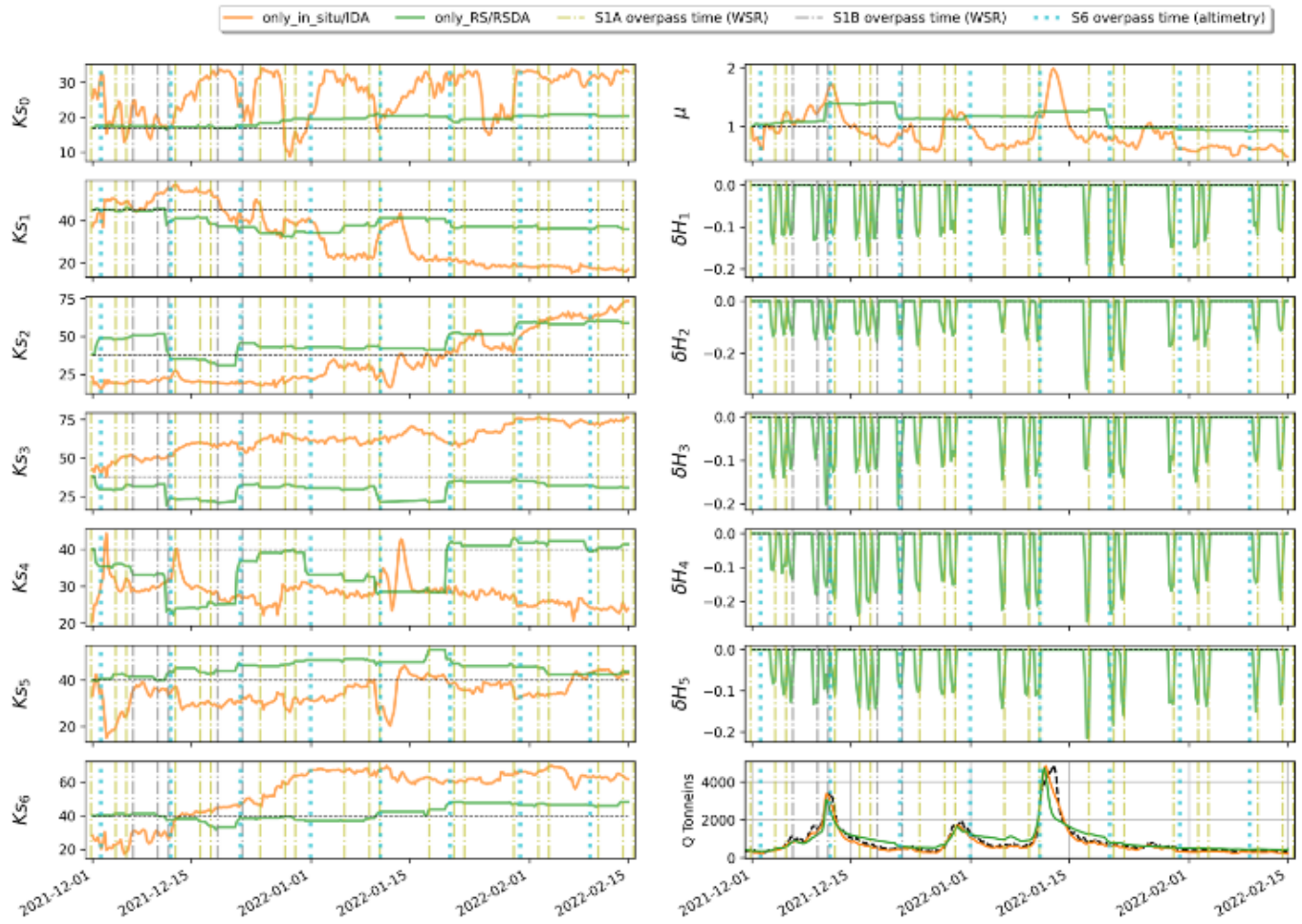



Figure 5. Evolution of controlled parameters for roughness, multiplicative correction to the inflow, and state correction in the floodplain.

*B. Results in the observation space: WLs at observing stations*

Table III Water level RMSE w.r.t. in-situ WL at VigiCrue observing stations. Lowest RMSE values are underlined.

| Exp. | RMSE [m] | | | |
|---|---|---|---|---|
| | **Tonneins** | **Marmande** | **La Réole** | **Couthures** |
| OL | 1.162 | 0.940 | 0.940 | 0.787 |
| IDA | <u>0.189</u> | <u>0.137</u> | <u>0.140</u> | <u>0.280</u> |
| RSDA | 0.810 | 0.990 | 0.886 | 0.647 |

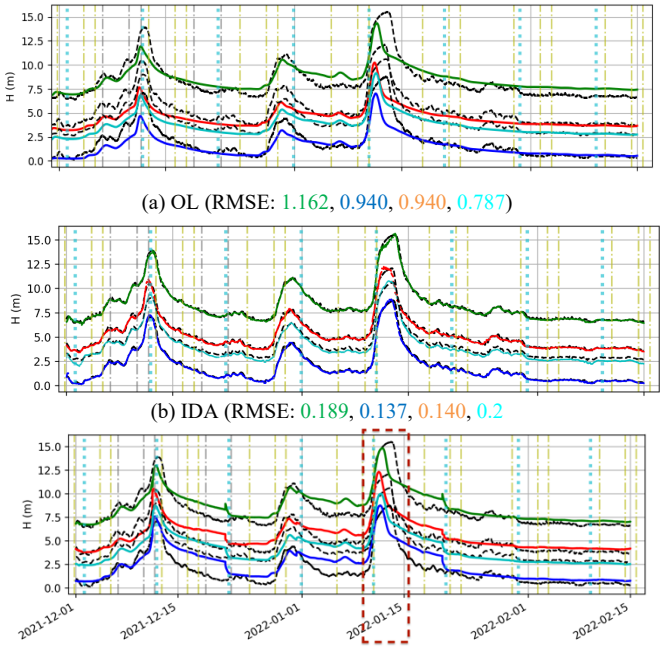
The root-mean-square errors (RMSE) computed over time for the 2021-2022 flood event using the WLs simulated by the experiments OL, IDA and RSDA, with respect to the observed WLs at observing stations are summarised in Table III. Figure 6 displays the WLs simulated by the different experiments, at Tonneins (red lines), Marmande (blue lunes), Couthures (cyan lines) and La Réole (green lines), in comparison to the corresponding observed WLs (black-dashed lines). It can be noted that the simulated WLs at different observing stations (either those used for assimilation, or that of Couthures used for validation only) are improved significantly in IDA (Figure 6b) compared to the OL experiment (Figure 6a) throughout the flood event; even though there is still a minor underestimation at Tonneins (red line) and La Réole (green line) by IDA compared to the observations near the third flood peak.

For RSDA (Figure 6c), with the contribution of RS data, only the WLs at the peaks are improved. This is due to a number of reasons. First, the S1-derived flood extent maps offer limited knowledge on the flow dynamics in the floodplain to correct the involved uncertainties. Second, during the period following a S6 pass at high flows (of which the respective S6 data was assimilated), the simulated WLs in the river still remain much higher than the observations, and hence causes higher misfits compared to the OL experiment. This stays until the next S6 pass (typically when it is of low flow) where the WLs are reduced and become similar to the observed WLs. The fact that the WLs are not consistently improved by the RSDA (compared to OL) can be underwhelming in general, regarding the merits of assimilating RS data without in-situ data. However, the improved peak WLs and the immediate correction of the WL overestimation at the next assimilation represent what RS data can offer in terms of uncertainty reduction at S6 assimilation times. This current limitation also advocates for the need of more frequent observations from space in order to improve the 10-day revisit frequency of the S6 satellite. It can be expected

that for a more significant flood event, the S1 observations shall satisfy such a need for a denser observing network, as shown in [3, 5].

### *C. Results in the observation space: WSE profiles along the river centreline*

Figure 7 shows the WSE profiles along the river centreline, from which the S6 data were measured. There are eight panels associated with eight S6 overpasses. The black-dashed lines represent the WSE profiles observed by the S6 satellite, whereas the WSE profiles simulated by the OL, IDA, and RSDA experiments are represented by the blue, orange and green lines, respectively. The curvilinear abscissa of the plots follows the flow direction, i.e., smaller abscissa is upstream of a greater abscissa. Three particular dates are noted "high flow" (with panel title in boldface), as they correspond to the three high-flow dates, namely 2021-12-12 (first peak of the event), 2021-12-31 (slightly after the second peak) and 2022-01-10 (before the third peak of the event).




(a) OL (RMSE: 1.162, 0.940, 0.940, 0.787)

(b) IDA (RMSE: 0.189, 0.137, 0.140, 0.2

(c) RSDA (RMSE: 0.810, 0.990, 0.886, 0.647)

Figure 6. Simulated WL compared to observations by (a) OL, (b) IDA and (c) RSDA.

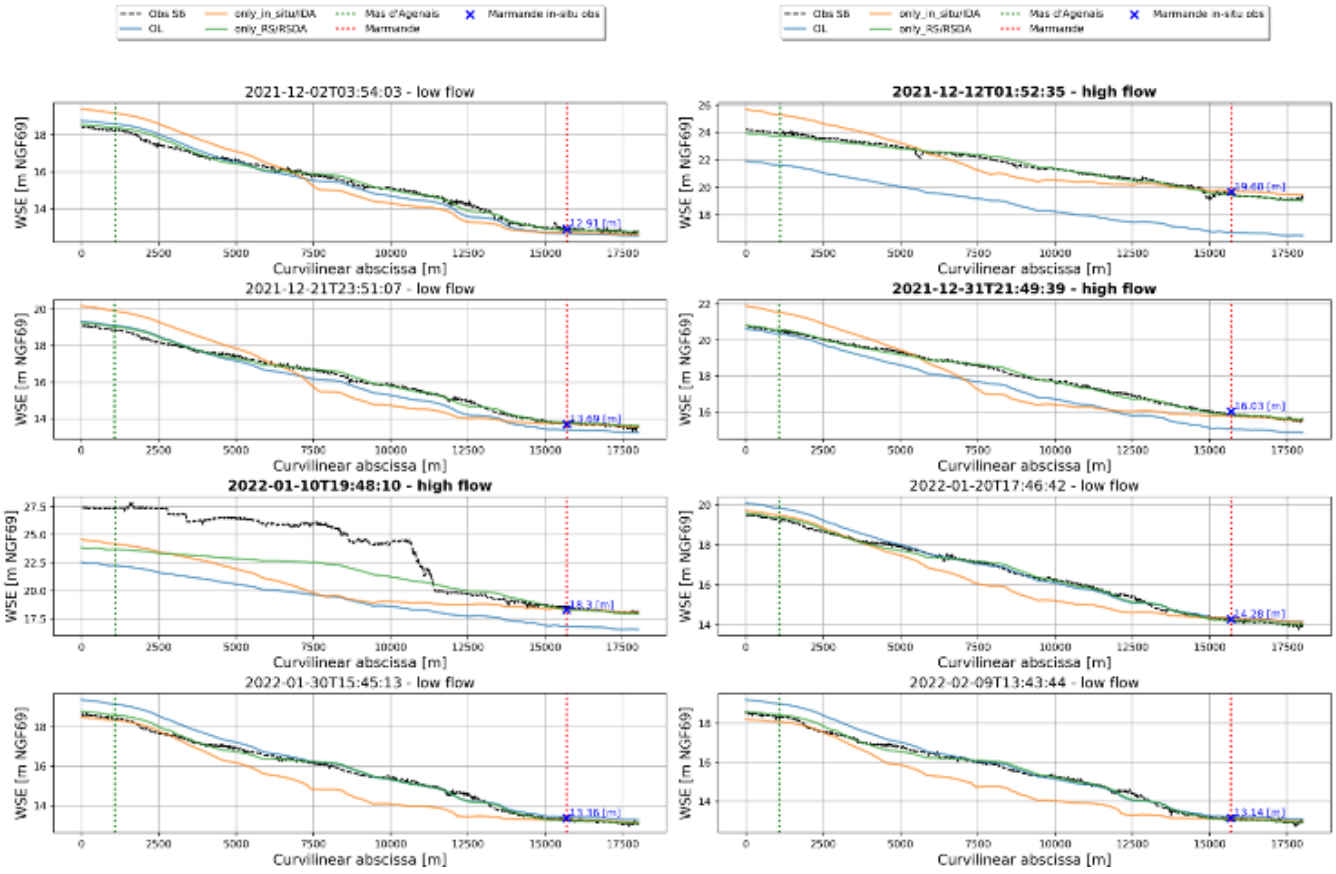



Figure 7. Simulated WSE at river centreline compared to S6-derived WSE observations.

The S6 measurements allow to validate experiments in high spatial density (up to 10 m in this work) that is not possible when using in-situ WL data. It reveals different outcomes yielded by one experiment to reveal at different segments of the river. For instance, OL experiment (blue lines) shows an underestimation of WSEs in one part of the profile and an overestimation in another on all eight overpasses. The underestimation became global and especially problematic on high-flow days, as shown by the gaps between the blue lines and black-dashed lines on these panels. It results in a gap of more than two metres at the first flood peak on 2021-12-12. In addition, after the third peak of the event, the WSEs yielded by OL show a slight overestimation over the left part of the profile (between the curvilinear abscissa 0 and 6,000 m). The area of observation by the S6 satellite over the studied catchment, despite covering only a part of it, is also interesting as it stretches to the Marmande in-situ station, where the local residents have been regularly impacted by flooding.

On most days, the WSEs along the river simulated by the IDA (orange lines) are coherent with the S6 observations over the right part of the profile (between the curvilinear abscissa 15,000 and 17,500 m). This is due to the fact that there is an observing station at Marmande, whose location along the curvilinear abscissa is represented by the vertical red-dotted line in Figure 7, around the curvilinear abscissa at 16,800 m. The in-situ WSEs measured at this station are shown by the blue crosses in each panel. Indeed, thanks to this assimilation, the resulting WSEs by IDA, in the vicinity of the in-situ station, stay very close to the observations. However, at positions along the river further away from the Marmande station, the WSEs simulated by IDA differ significantly from the observed WSEs. Underestimated WSEs at the middle part of the profiles by IDA are also a common problem, as shown throughout the flood event with the orange lines far below (more than one metre) the black-dashed lines.

Considering the RSDA experiment (green lines), as one can expect, the simulated WSEs along the river are quite consistent throughout the event, with slightly underperformances at high-flow dates. Moreover, the S6 measurements on 2022-01-10 present a part of the observation (i.e., between the abscissa 0 and 10,000 m) being erroneous due to a false initiation problem with the Fully-focused SAR processing. This error can be easily diagnosed when analysing the OL/IDA WSEs on this day. In this work, a process of quality control has been applied on RSDA to reject those erroneous S6 observations from the assimilation. This results in RSDA (green line) taking into account only partially the observations on 2022-01-10. This rejection of misfits demonstrates the flexibility of the performed DA strategy regarding errors with large magnitudes. However, this contributes to the simulated peak WLs at observing stations different from each other. As such, back in Figure 6, the peak WLs following this S6 overpass (shown by the red rectangle) from RSDA shows a similar height for Tonneins (red line) and Marmande (blue line) compared to their respective observed peak, but it exhibits smaller peaks for Couthures (cyan line) and La Réole (green line), hence creates larger misfits for these two downstream stations. This is because the part of the S6 observations near Marmande that are not rejected in the DA.

It should be reemphasized that, as mentioned in the previous subsection, the fact that there is only one S6 overpass every 10 days imposed the controlled parameters to remain the same even for several days after the assimilation. This was the reason why the WLs within the river or at the observing stations have the tendency to stay much higher than the observed WLs. This situation is even more severe when only a part of the observations (i.e., the 2022-01-10 incident) is taken into account for the DA.

### *D. Results in the observation space: WSR in the floodplain*

Figure 8 displays the S1-derived WSR (black lines) at S1 overpass times and the WSR computed for OL (blue lines), IDA (orange lines) and RSDA (green lines) experiments over the five subdomains of the floodplain. As aforementioned, the observed flood extent maps derived from S1 SAR image present little water surfaces in the floodplain. This is due to the fact that the S1 images were acquired during relatively low flow dates, and right before the third peak of the flood event occurred, one of the two S1 satellites (Sentinel-1B, shown by yellow dash-dotted vertical line in Figure 4) became defected. This reduced the S1 observation capacity by a half after mid-December 2021. In Figure 8, the black lines show the observed WSRs that are almost zeros throughout the event. These lines are overlapped by the blue lines that represent the OL experiment, which shows underestimation of the flood extent due to the low forcing discharge simulated by the ISBA-CTRIP hydrologic model. Therefore, its resulting WSRs are similar to the observed ones. When only in-situ data was assimilated (in IDA), the WSRs over the different floodplain subdomain are much higher than the observed WSRs. Such an overestimation starts around the third peak for the first three subdomains ($\delta H_{1,2,3}$), whereas this was the case since the beginning of the flood for the downstream subdomains ($\delta H_4$ and $\delta H_5$).

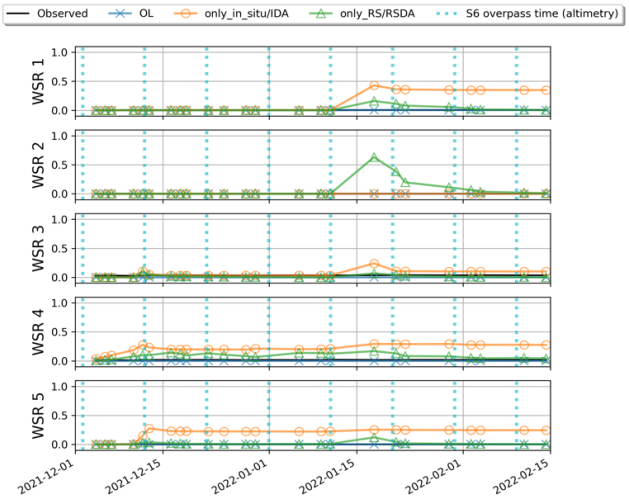



Figure 8. Simulated and observed WSR values in the five floodplain zones.

The assimilation of RS data by RSDA (S1 for the WSRs in the floodplain and S6 for the WSEs along the river) yields WSRs more coherent to the observations derived from S1 images, especially in the subdomain 3 and 5. The $\delta H_2$ subdomain (which is significantly smaller compared to the

other subdomains), however, has been overestimated at the third flood peak. This could stem from the rejection and non-assimilation of the erroneous S6 measurements on 2022-01-10 (between the abscissa 0 and 10,000 m as mentioned above) which led to the RSDA experiment keeping the same friction coefficient at the corresponding river segment, i.e., $Ks_2$ at the fourth and fifth S6 overpasses (vertical cyan lines). On the other hand, the WSR associated with the δH4 subdomain still is overestimated even though the state correction in this zone is active the whole event.

## V. Conclusions and Perspectives

This study presents the merits of assimilating 2D flood extent observations derived from remote sensing Sentinel-1 SAR images and Sentinel-6-Michael Freilich altimetry data with an Ensemble Kalman Filter implemented on a hydrodynamic TELEMAC-2D model. The flood extent information from S1 SAR images is expressed in terms of Wet Surface Ratio or WSR computed over defined sensitive subdomains of the floodplain, whereas the altimetry data from S6 are obtained as WSEs over the river centreline every 10 days. The S6 observations cover nearly half of the studied catchment. The S1-derived WSRs are assimilated jointly with the S6 altimetry data, and its results were compared against the case when only in-situ water level observations were assimilated. The study was carried out over the Garonne Marmandaise catchment, focusing on the flooding event in December 2021-January 2022 when both types of satellite observation were available. Three experiments were realised; one in open-loop mode and two others in DA mode. The control vector gathers friction and forcing correction, and is augmented with correction of the hydraulic state in subdomains of the floodplain. All of the DA experiments were implemented by a cycled EnKF with an 18-hour assimilation window sliding with 6-hour overlapping. The simulation results were comprehensively assessed with 1D and 2D metrics with respect to assimilated data.

The first DA experiment IDA involves only in-situ observations whereas the other one RSDA assimilates both WSR observations derived from S1 2D flood extent maps and WSE observations from the S6 altimetry data. While both DA experiments focus on the sequential correction of friction coefficients and inflow discharge, RSDA additionally handles a dual state-parameter estimation within the EnKF, by treating inflow discharge and friction coefficients as well as the hydraulic state variable in five particular floodplain subdomains, representing evapotranspiration and/or ground infiltration processes that are unavailable in the TELEMAC-2D model. This difference was due to the availability of S1-derived observations (i.e., WSR) of the floodplain that involves only RSDA.

It has been shown that the assimilation of in-situ data in IDA significantly improves the simulation in the river bed, especially when there is a significant amount of uncertainty involving the upstream discharge provided by ISBA-CTRIP. The water levels at observing stations simulated by RSDA suggest that without in-situ data it is nearly impossible to compensate for such an underestimated discharge, even though the WSEs along the rivers have been improved significantly at times. Nevertheless, IDA overestimates the flow dynamics in the floodplain as shown by the WSRs in the five floodplain subdomains. Indeed, the in-situ observations located in the river bed, do not provide information on the dynamics in the floodplain. Previous works [3, 4, 18] have shown that the assimilation of RS data is beneficial when an observed discharge was used as forcing data, but in order to account for hydrologically-modelled forcing discharge, in-situ data is essential.

On the other hand, S6 data assimilation allows to substantially improve the WLs (both at observing stations and along the observed river segment) whenever there are observations available for assimilation, with a fine spatial resolution of the WSE in the river. The added value from S6 altimetry data regarding the dense WSE profile along the river allows to diagnose in fine detail the behaviour of the simulated WSEs, varying between the part near an observing station and those far away from it. This beneficial feature will be even more advantageous for a large-swath altimetry satellite like the recently launched SWOT that provides WSEs from the river as well as from the floodplain. This study validated the assertion that a densification, in time and space, of the observing network, especially in the floodplain with remote sensing data and advanced DA strategy, allows to improve the representation of the dynamics of the flow in the floodplains. In addition, the necessity of in-situ data has been reemphasized, especially when there are high amounts of uncertainties to be dealt with, e.g., underestimated discharge provided by a large-scale hydrologic model. Lastly, this work advocates for the multi-source data assimilation strategy implemented on top of a chained hydrologic-hydraulic model, making the most out of Earth Observation heterogeneous data. Such a diverse combination between models and observations, aiming at new observing strategies, heralds towards a Digital Twin framework in hydrology.

## Acknowledgement

This work was supported by CNES, CERFACS and SCO-France. The authors gratefully thank the EDF R&D for providing the Telemac-2D model for the Garonne River, and the SCHAPI, SPC Garonne-Tarn-Lot and SPC Gironde-Adour-Dordogne for providing the in-situ data.

## References

[1] Fekete, B. M., Looser, U., Pietroniro, A., & Robarts, R. D. (2012). Rationale for monitoring discharge on the ground. Journal of Hydrometeorology, 13(6), 1977-1986.

[2] Nguyen, T. H., Ricci, S., Piacentini, A., Bonassies, Q., Suquet, R. R., Luque, S. P., ... & David, C. (2023). Reducing Uncertainties of a Chained Hydrologic-hydraulic Model to Improve Flood Forecasting Using Multi-source Earth Observation Data. arXiv preprint arXiv:2306.10059.

[3] Nguyen, T. H., Ricci, S., Piacentini, A., Fatras, C., Kettig, P., Blanchet, G., ... & Baillarin, S. (2022). Dual State-Parameter Assimilation of SAR-derived Wet Surface Ratio for Improving Fluvial Flood Reanalysis. Water Resources Research, vol. 58, no. 11, p. e2022WR033155, 2022. e2022WR033155 2022WR033155.

[4] Nguyen, T. H., Ricci, S., Piacentini, A., Suquet, R. R., Blanchet, G., Luque, S. P., & Kettig, P. (2022). Enhancing Flood Forecasting with Dual State-Parameter Estimation and Ensemble-based SAR Data Assimilation. TELEMAC-MASCARET User Conference 2022, Paris-Saclay, 297-305.

[5] Nguyen, T. H., Ricci, S., Piacentini, A., Simon, E., Suquet, R. R., & Luque, S. P. (2023). Dealing With Non-Gaussianity of SAR-derived Wet

Surface Ratio for Flood Extent Representation Improvement. arXiv preprint arXiv:2306.08466.

[6] Munier, S., & Decharme, B. (2022). River network and hydro-geomorphological parameters at 1/12° resolution for global hydrological and climate studies. Earth System Science Data, 14(5), 2239-2258.

[7] Hervouet, J. M. (2007). Hydrodynamics of Free Surface Flows: Modelling with the Finite Element Method. John Wiley & Sons.

[8] Decharme, B., Delire, C., Minvielle, M., Colin, J., Vergnes, J. P., Alias, A., ... & Voldoire, A. (2019). Recent changes in the ISBA-CTRIP land surface system for use in the CNRM-CM6 climate model and in global off-line hydrological applications. Journal of Advances in Modeling Earth Systems, 11(5), 1207-1252.

[9] Noilhan, J., & Planton, S. (1989). A simple parameterization of land surface processes for meteorological models. Monthly Weather Review, 117(3), 536-549.

[10] Oki, T., & Sud, Y. C. (1998). Design of Total Runoff Integrating Pathways (TRIP)—A global river channel network. Earth Interactions, 2(1), 1-37.

[11] Decharme, B., Alkama, R., Papa, F., Faroux, S., Douville, H., & Prigent, C. (2012). Global off-line evaluation of the ISBA-TRIP flood model. Climate Dynamics, 38(7), 1389-1412.

[12] Besnard, A., & Goutal, N. (2011). Comparison between 1D and 2D Models for Hydraulic Modeling of a Floodplain: Case of Garonne River. La Houille Blanche-Revue Internationale De L'Eau, (3), 42-47.

[13] Gauckler, P. (1867). Etudes Théoriques et Pratiques sur l'Ecoulement et le Mouvement des Eaux. Gauthier-Villars.

[14] Dinardo, S., Maraldi, C., Cadier, E., Rieu, P., Aublanc, J., Guerou, A., ... & Scharroo, R. (2023). Sentinel-6 MF Poseidon-4 Radar Altimeter: Main Scientific Results from S6PP LRM and UF-SAR Chains in the First Year of the Mission. Advances in Space Research.

[15] Egido, A., & Smith, W. H. (2016). Fully Focused SAR Altimetry: Theory and Applications. IEEE Transactions on Geoscience and Remote Sensing, 55(1), 392-406.

[16] Nguyen, T. H., Ricci, S., Fatras, C., Piacentini, A., Delmotte, A., Lavergne, E., & Kettig, P. (2022). Improvement of Flood Extent Representation with Remote Sensing Data and Data Assimilation. IEEE Transactions on Geoscience and Remote Sensing, 60, 1-22.

[17] Nguyen, T. H., Ricci, S., Piacentini, A., Simon, E., Rodriguez Suquet, R., & Pena Luque, S. (2023). Gaussian Anamorphosis for Ensemble Kalman Filter Analysis of SAR-derived Wet Surface Ratio Observations. arXiv preprint arXiv:2304.01058.

[18] Ricci, S., Nguyen, T. H., Le Gac, S., Boy, F., Piacentini, A., Rodriquez-Suquet, R., Pena Luque, S., et al. (2023). Comparisons and Water Level Analyses using Sentinel-6MF Satellite Altimetry Data with 1D Mascaret and 2D Telemac Models. EGU General Assembly 2023, no. EGU23-6513.